Catal Lett (2012) 142:1498–1504
DOI 10.1007/s10562-012-0893-2

Studies of the Catalytic Oxidation of CO Over Ag/CeO_2 Catalyst

Yan Kang · Min Sun · Aimin Li

Received: 20 May 2012 / Accepted: 14 August 2012 / Published online: 18 September 2012

Abstract CO oxidation was investigated over Ag/CeO_2 and CeO_2 catalysts prepared by sol–gel method in this work. The catalytic activity of Ag/CeO_2 was higher than pure CeO_2. The chemico-physical properties of catalysts were characterized by XRD, TEM, XPS, H_2-TPR and Raman spectroscopy. The characterization results indicated that a part of silver was inserted into the lattice of CeO_2 and aroused the expansion of lattice. Raman studies of Ag/CeO_2 demonstrated that the concentration of oxygen vacancies greatly increased at 5 vol.% CO/N_2 atmosphere and gradually decreased at O_2 atmosphere with the rising temperature from 30 to 300 °C respectively. However, a different behavior was observed over pure CeO_2. The obtained Raman results showed that the oxygen storage capability of Ag/CeO_2 was superior to that of CeO_2 and larger amount of lattice oxygen of the former took part in the oxidation reaction evidenced by changes of oxygen vacancy. On the basis of characterization data, it was proposed that the introduction of Ag into CeO_2 facilitated the activation of lattice oxygen and formation of oxygen vacancies. These features may be responsible for the higher catalytic activity of Ag/CeO_2 for CO oxidation.

Y. Kang (✉)
Research Center of Analysis and Test, East China University of Science & Technology, Shanghai 200237, China
e-mail: kangyanhuda@163.com

M. Sun (✉)
Lab for Advanced Materials, Research Institute of Industrial Catalysis, East China University of Science & Technology, Shanghai 200237, China
e-mail: sunmin20025826@163.com

A. Li
Shanghai Institute of Ceramics, Chinese Academy of Sciences, Shanghai 200050, China

Keywords CO oxidation · Ag/CeO_2 · Oxygen vacancy · Raman

1 Introduction

Catalytic oxidation of CO has been an important subject in recent years, which has wide applications in different fields, including purification of environmental gas, treatment of exhaust gas from automobiles and selective oxidation of CO in reformer gas for fuel cell and so on.

Ceria (CeO_2) has been used as a principal oxide support in catalytic oxidation of CO due to its remarkable oxygen storage capability (OSC) and redox ability. These properties originated from its easy creation and diffusion of oxygen vacancies, especially at the surface [1]. It was pointed out that the presence of oxygen vacancies was able to provide sites for oxygen activation and increase the diffusion rate of oxygen [2]. In order to enhance the oxygen vacancy levels, the doping of ceria has been an efficient method, which can result in the formation of defective fluorite structure [3, 4]. Rare earth metals and transition metals were frequently employed for this purpose [5–13]. Chen et al. [14] investigated the mechanism of CO oxidation on Fe-modified CeO_2 using periodic density functional theory calculations and found that the addition of Fe promoted the formation of oxygen vacancies.

Supported silver catalysts have been investigated recently [15–18]. Imamura et al. [19] studied the catalytic activity of Ag/CeO_2 and concluded that the high dispersion of silver helped to maintain the high activity for CO oxidation. Sarode et al. [20] investigated the local environment of Ag in Ag/CeO_2 by extended X-ray absorption fine structure spectroscopy and found that Ag^+ like species was

presented. Scirè et al. [21] reported a comparative study on ceria supported group IB metal catalysts and proposed that a higher atomic radius of the IB metal and the presence of smaller crystallites of both IB metal and ceria resulted in a larger enhancement of reactivity of surface oxygen on ceria. Hegde et al. [22] reported that Ag seemed to be ionically dispersed on CeO_2 crystallites and surface concentration of Ag was much higher than bulk. Among these studies, the mechanism of CO oxidation over Ag/CeO_2 is still under debate. The roles of silver and ceria support have not been extensively explored about this system. In this work, the catalytic oxidation mechanism of CO over Ag/CeO_2 was systematically studied with the aim to obtain more information. The correlation among silver nanoparticles, support and catalytic activity is addressed via experimental measurements. It was proposed that the introduction of Ag enhanced the OSC of Ag/CeO_2 catalyst and favored the generation of oxygen vacancies and activation of lattice oxygen. These features may be mainly responsible for the better catalytic performance of Ag/CeO_2 catalyst.

2 Experimental

2.1 Catalyst Preparation

Ag/CeO_2 catalyst (Ag/Ce = 0.1) was prepared by a sol–gel method. An appropriate amount of $AgNO_3$, $Ce(NO_3)_3$ and citric acid were dissolved into de-ionized water. The mixed solution was evaporated under stirring until the transparent gel was formed. The resulting gel was dried at 100 °C for 2 h, followed by the decomposition at 450 °C for 2 h to remove organics and the final calcinations at 600 °C for 3 h under static air. After grinding, the catalyst powder was obtained and the loading of Ag was about 6 wt.%.

2.2 XRD, H_2-TPR, TEM, XPS, BET and Raman

The X-ray powder diffraction (XRD) analysis was performed on a Bruker D8 powder diffractometer using a Cu Kα radiation (40 kV and 40 mA). The diffractograms were recorded in the 2θ range of 10–80° with a 2θ step size of 0.02° and a scanning speed of 6° min^{-1}. Rietveld refinements were carried out with the program Jade 5.0 and the average crystal size was determined by the Scherrer's equation. Hydrogen temperature programming reduction (H_2-TPR) measurements were carried out using a commercial temperature programming system. 30 mg catalyst was heated in the flow of 5 vol.% H_2/N_2 (45 mL min^{-1}) at a heating rate of 10 °C min^{-1} from 100 °C to 800 °C. The amount of H_2 uptake during the reduction was measured by thermal conductivity detector (TCD).

The BET surface areas of the samples were measured on a Micromeritics ASAP 2020 instrument by N_2 adsorption at −196 °C. The samples were degassed at 120 °C and 1×10^{-4} Pa for 10 h before the measurements.

Transmission electron microscopy (TEM) images of the catalysts were recorded on a JEOL JEM-2100 microscope operating at 200 kV. The samples were dispersed in ethanol and kept in an ultrasonic bath for 15 min, then deposited on a carbon-covered copper grid for each measurement.

X-ray photoelectron spectra of the catalysts were recorded on Kratos Axis Ultra DLD surface analysis instrument using an Al Kα radiation (1,484.6 eV) as primary excitation. The binding energies were calibrated by C_{1s} (284.8 eV). XPS elemental spectra were acquired in the fixed analyser transmission (FAT) mode with 0.1 eV energy steps at a pass energy of 40 eV. The samples were pressed into thin discs and mounted on a sample rod.

Raman measurements were performed on a Renishaw invia Raman spectroscope using a 300 mW 785 nm laser as the excitation source with a dwell time of 10 s and number of scans of 1. The microscope used a 50× objective and 1,200 g mm^{-1} grating. Raman measurements during the reaction processes were carried out on a Linkam THMS 600 thermal cell, coupled to the Raman equipment. The cell allowed the use of controlled atmosphere and temperature. The flowing gas used in Raman measurements was 5 vol.% CO/N_2 and O_2 (99.99 %). About 10 mg sample was pressed into a slice (diameter 5 mm) and inserted into the cell. Then the cell was heated from room temperature to 300 °C with a heating rate of 10 °C min^{-1} under a gas flow. Each spectrum was collected after the sample was held for 5 min at the desired temperature point under the flow. Finally, the sample was cooled to room temperature.

2.3 Catalytic Activity Evaluation

The CO oxidation reaction was performed in a conventional continuous flow fixed-bed microreactor. The catalyst (50 mg) was evenly mixed with 100 mg SiO_2 granules (0.3–0.5 mm) to reduce the pressure drop and packed into the reactor. Before reaction, the catalyst did not undergo any pretreatments. The reaction was carried out at a heating rate of 5 °C min^{-1} up to the chosen temperature and the sample was held for 5 min at the desired temperature point from room temperature to 300 °C. The reactant flow consisted of a mixture of 5,000 ppm CO (10 mL min^{-1}) and air (40 mL min^{-1}). The mixture with a total gas flow of 50 mL min^{-1} was fed to the reactor at atmospheric pressure and passed over the catalysts for 20 min. The effluent gases were analyzed on-line by a gas chromatograph equipped with a FID detector.

3 Results and Discussion

3.1 The Catalytic Performance of CeO_2 and Ag/CeO_2 for CO Oxidation

Figure 1 displays the CO conversion as a function of reaction temperature for pure CeO_2 and Ag/CeO_2 catalysts. As shown in Fig. 1, no significant CO conversion was observed when the reaction temperature increased to 140 °C and this value was below 10 % even when the temperature reached 300 °C on the bare CeO_2. Compared to the pure CeO_2, Ag/CeO_2 was more active. A remarkable increase of CO conversion on Ag/CeO_2 was observed up to 180 °C and the complete conversion was achieved at 250 °C. These results revealed that the Ag/CeO_2 displayed much better catalytic behavior toward CO oxidation than CeO_2, indicating that the presence of Ag greatly enhanced the catalytic activity.

3.2 XRD

The XRD patterns of CeO_2 and Ag/CeO_2 are presented in Fig. 2. The profile of the bare ceria reveals the presence of diffraction peaks related to CeO_2 phase in the cubic crystal structure of fluorite type. The average particle size of the CeO_2 was calculated to be around 20 nm according to the Scherrer's equation, and this value was confirmed by TEM. Compared to the pattern of CeO_2, two additional weak peaks at about 38.2° and 44.2° were observed on the Ag/CeO_2 catalyst, which were ascribed to the diffraction peaks of Ag (111) and Ag (200) [19, 21]. The average diameters of silver and ceria particles calculated by the Scherrer's equation were 16 and 15 nm respectively. Considering that the peak at 38.2° can be attributed to both Ag and Ag_2O species, it must be pointed out that the presence of Ag_2O can't be fully excluded. However, according to the discussion of XRD in literature [21], metallic Ag species predominated over Ag_2O in Ag/CeO_2 catalyst in this work.

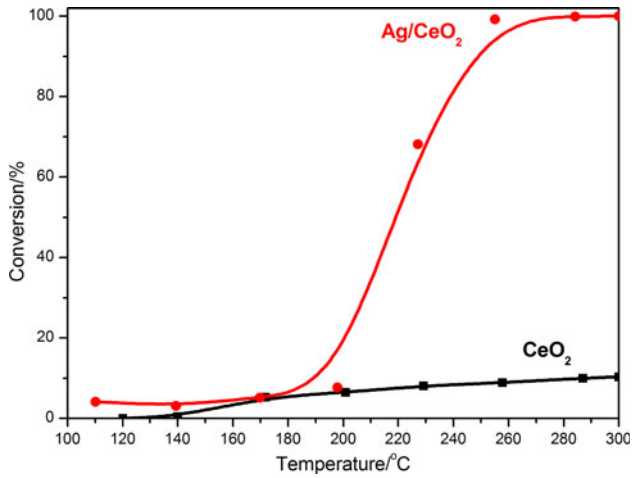

Fig. 1 Comparison of CO oxidation activities of CeO_2 and Ag/CeO_2 catalysts

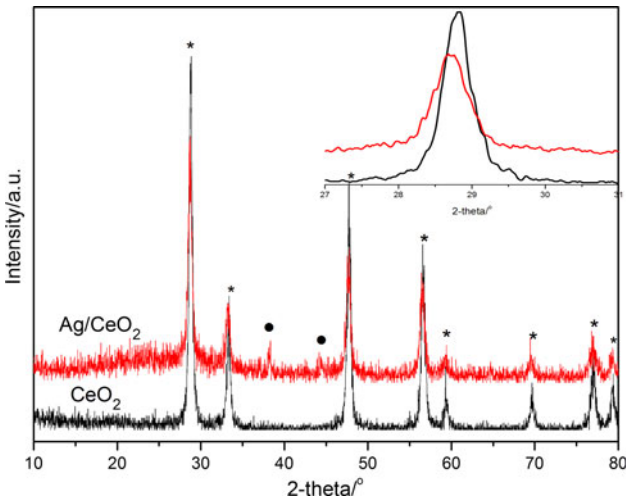

Fig. 2 The powder XRD patterns of catalysts: **a** CeO_2 and **b** Ag/CeO_2 (*asterisk* ceria, *black circle* silver)

As shown in the insert of Fig. 2, it could be seen that the diffraction peak at 28.5° on Ag/CeO_2 catalyst shifted to lower angle compared to that of pure CeO_2, which suggested that a part of Ag incorporated into the lattice of CeO_2 and aroused the expansion of the lattice [6, 7]. The inserted Ag increased the crystal defects of CeO_2, which might accelerate the activation of lattice oxygen in the reaction. The particle sizes and surface areas of catalysts are presented in Table 1. It could be seen that the size of Ag particles from TEM was 18 nm, which was slightly larger than the value from XRD in Ag/CeO_2. In addition, the particle size of CeO_2 estimated from XRD was similar to the value from TEM.

3.3 TPR

Figure 3 shows the TPR profiles of pure CeO_2 and Ag/CeO_2 catalysts. In the examined temperature range (40–800 °C), pure CeO_2 exhibits two well resolved reduction peaks. One centered at 510 °C and the other was above 790 °C. The former one belonged to the reduction of the surface capping oxygens of ceria [6, 23, 24], while the latter one, more intense, was ascribed to the reduction of

Table 1 The chemico-physical properties of catalysts

Sample	Average diameter from XRD (nm)	Average diameter from TEM (nm)	BET surface area ($m^2\ g^{-1}$)	Content (%)
CeO_2	20	21	32	–
Ag/CeO_2	16/15	18/16	45	6

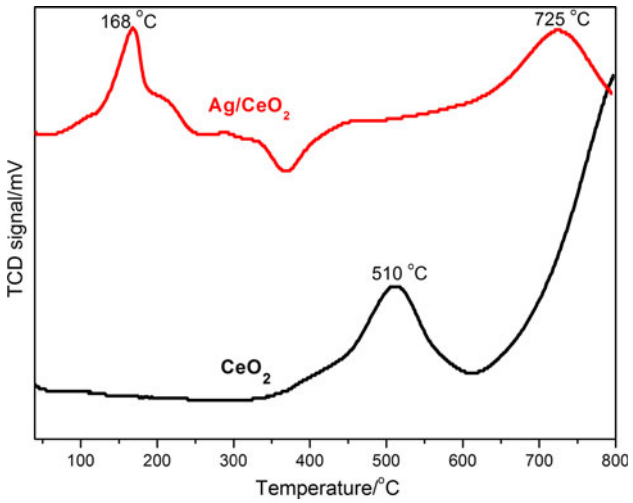

Fig. 3 TPR profiles of CeO_2 and Ag/CeO_2 catalysts

bulk oxygen of ceria [25]. For Ag/CeO_2 sample, two main reduction peaks were observed. The first one around 168 °C could be assigned to the reduction of surface capping oxygen of ceria interacting with silver species [6, 20]. An obvious shift of the reduction peak toward lower temperature was due to the interaction between silver and ceria. It was indicated that the presence of silver improved the reducibility of surface oxygen on CeO_2 and facilitated the oxygen transfer across the solid–gas interface during reaction [26]. The second one at 725 °C was attributed to the reduction peak of bulk oxygen of ceria. The TPR results showed that the presence of silver significantly improved the reducibility of surface capping oxygen of ceria.

3.4 TEM

TEM measurements were carried out in order to obtain the particle sizes and morphologies of catalysts. As indicated in Fig. 4a, the CeO_2 crystallized in a cubic shape with particle size being around 21 nm. The *d* spacing for the lattice was 0.313 nm, which corresponded to the CeO_2 (111) lattice plane of the cubic cell [27, 28]. In the case of Ag/CeO_2 sample, the average sizes of Ag and CeO_2 particles were around 18 and 16 nm respectively (Fig. 4b). The *d* spacing of Ag was 0.204 nm, which was corresponding to the Ag (200) [29].

3.5 XPS and BET

XPS spectrum of Ag_{3d} electron is presented in Fig. 5. The binding energy of Ag ($3d_{5/2}$) peak was at 367.7 eV. Compared to Ag metal, a lower shift of the Ag_{3d} binding energy was observed, which demonstrated the presence of +1 state of Ag [17, 21, 30]. The peak curve could be fitted into a pair of peak with binding energies of 367.6 and 368.1 eV, which were attributed to Ag^+ and neutral Ag atom, respectively [31–33].

The BET surface areas of CeO_2 and Ag/CeO_2 were 32 and 45 $m^2\ g^{-1}$ respectively (Table 1). An increase in the specific surface area (compared to the pure CeO_2) may be due to the evolution of a new porosity by the introduction of Ag into the CeO_2 structure and small Ag nanoparticle on the surface of ceria [7].

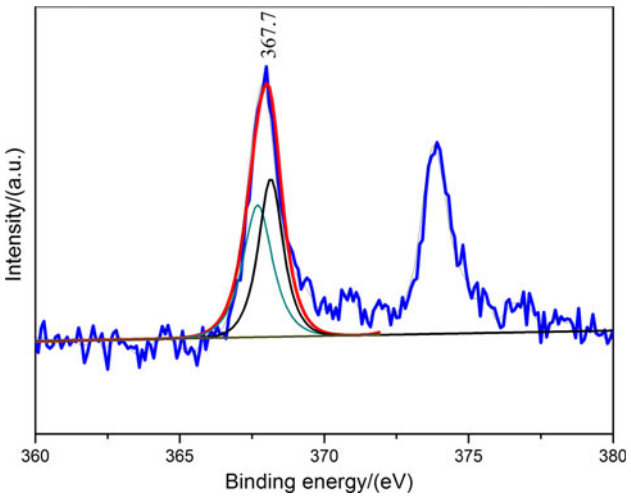

Fig. 5 XPS spectra of the Ag(3d) core level in Ag/CeO_2

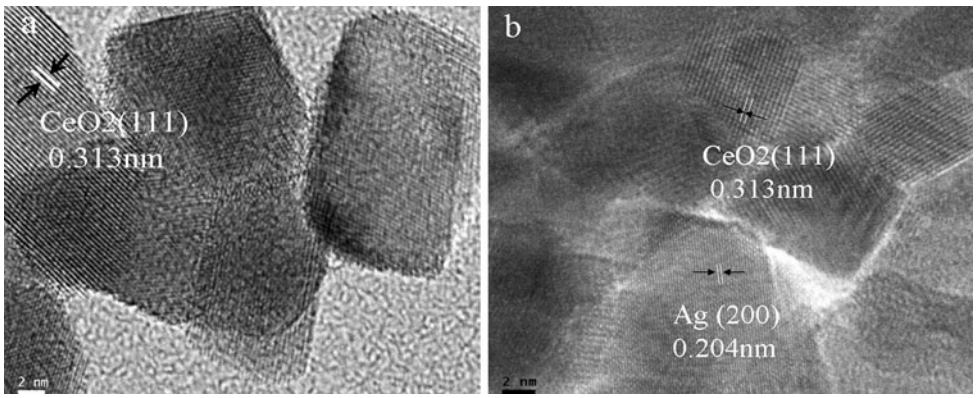

Fig. 4 TEM images of CeO_2 and Ag/CeO_2 catalysts

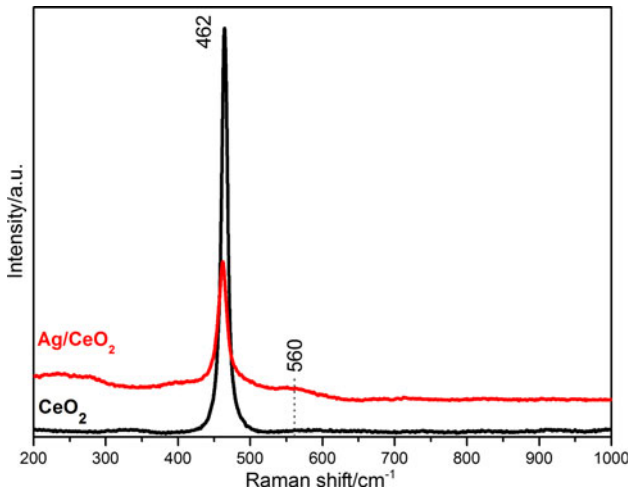

Fig. 6 Raman spectra of CeO_2 and Ag/CeO_2

3.6 Raman

Figure 6 shows the Raman spectra of pure CeO_2 and Ag/CeO_2 catalysts. The main band at 462 cm^{-1} was assigned to the F_{2g} vibration mode of fluorite structure of CeO_2 [34]. For Ag/CeO_2 catalyst, there is an additional band centered at 560 cm^{-1}, which was ascribed to the oxygen vacancies in the CeO_2 [12, 35]. The generation of oxygen vacancies was due to the incorporation of Ag into the lattice of ceria [5]. Moreover, there was a small variation in the Raman shift of F_{2g} mode of the two samples. This shift should be related to the change of the M–O vibration frequency after incorporation with Ag [36, 37]. Therefore, these Raman results indirectly confirmed the interaction between Ag and the CeO_2 support.

Raman spectra during the reaction processes were also recorded in order to obtain surface information of catalysts.

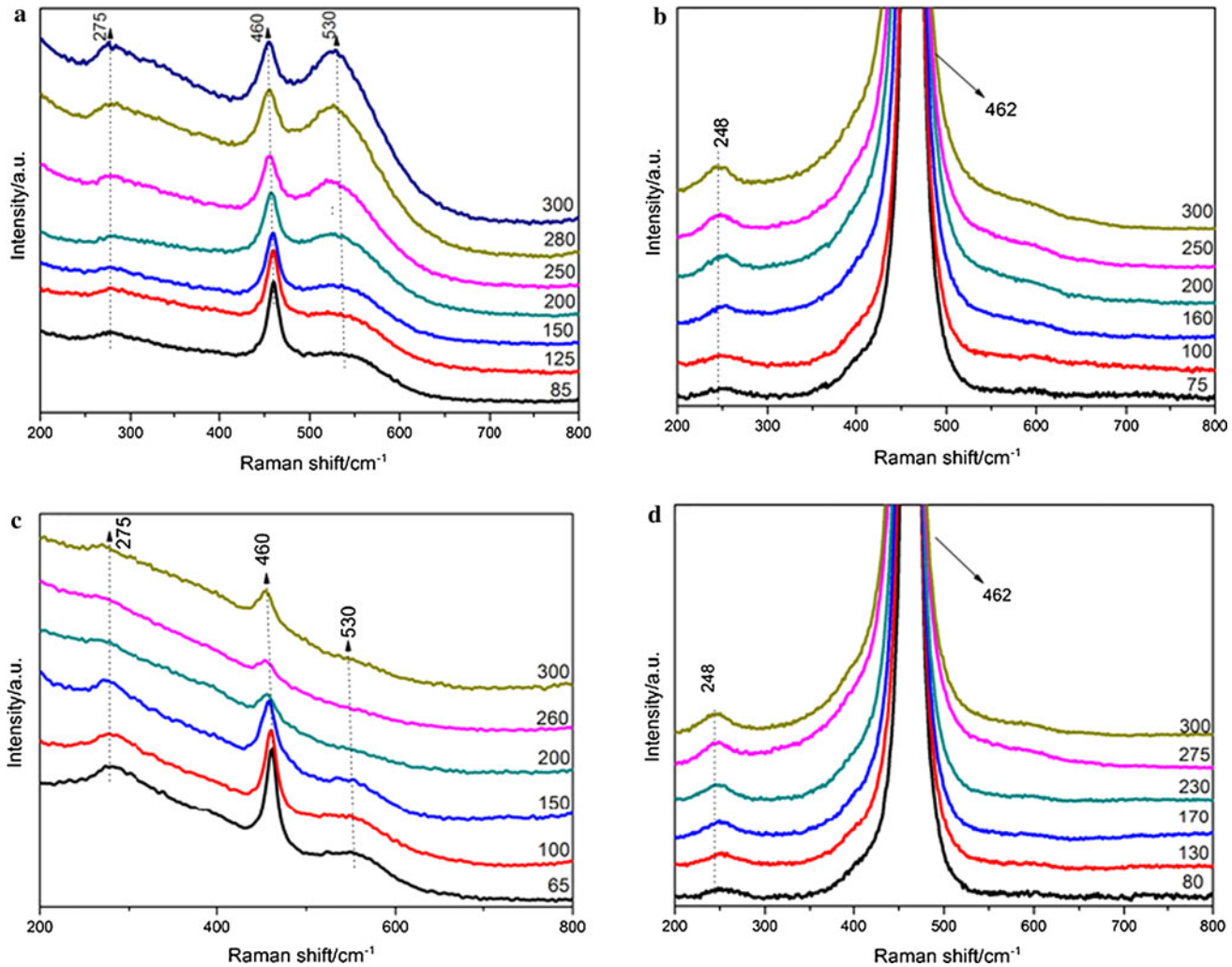

Fig. 7 Raman spectra of different catalysts under different reaction conditions (**a** Ag/CeO_2—5 vol% CO/N_2, **b** CeO_2—5 vol% CO/N_2, **c** Ag/CeO_2–O_2, **d** CeO_2–O_2)

Figure 7 shows the Raman spectra of CeO_2 and Ag/CeO_2 in 5 vol.% CO/N_2 and O_2 atmospheres at different temperature points. As shown in Fig. 7a, three bands at 275, 460 and 530 cm^{-1} were observed on the spectra of Ag/CeO_2 catalyst under 5 vol.% CO/N_2 flow. It has been reported that the Raman band at 246 cm^{-1} over $Ce_{0.67}Zr_{0.33}O_2$ was ascribed to the oxygen vacancy [38]. Meanwhile, the changing trend of the band at 275 cm^{-1} was consistent with that of the peak at 530 cm^{-1} in this work. Hence, it was reasonable to assign the band at 275 cm^{-1} to the oxygen vacancies. It could be seen from Fig. 7a that the intensity of the peak at 530 cm^{-1} significantly increased with the rising temperature and this peak could still be obviously observed after the sample was cooled to room temperature (data not shown). Generally, the ratio between the areas of bands at 530 (A_{530}) and 460 cm^{-1} (A_{460}) is a measurement of the number of oxygen vacancies in the material, in such a way that the higher the A_{530}/A_{460} value, the higher the number of oxygen vacancies were [7, 39]. As shown in Fig. 7a, it was found that the ratio of A_{530}/A_{460} significantly increased under CO flow with the rising temperature. However, the Raman peak at 530 cm^{-1} hardly appeared on the spectra of CeO_2 at the same conditions (Fig. 7b), suggesting that there were higher amount of oxygen vacancies in the Ag/CeO_2. This, in turn, also indicated that CO oxidation consumed lattice oxygen of CeO_2, leading to the formation of surface oxygen vacancy in the 5 vol.% CO/N_2 flow. This consumption of lattice oxygen of CeO_2 over Ag/CeO_2 may be related to the weak binding between the oxygen atoms and the ceria [40]. Compared the Raman spectra of two samples, it was strongly suggested that the inserted Ag facilitated the breaking of bond between Ce–O and the release of lattice oxygen, which is in agreement with the Mars–van Krevelen (MVK) mechanism [41].

Nevertheless, the Raman spectra were very different when the Ag/CeO_2 catalyst was exposed to O_2 atmosphere (Fig. 7c). For Ag/CeO_2 catalyst, the intensity of the bands ascribed to oxygen vacancies gradually decreased with the increase of temperature, almost disappearing at 200 °C. However, as shown in Fig. 7d, the feature bands of pure CeO_2 in O_2 atmosphere were similar to that in CO/N_2 atmosphere. It was obvious that the presence of Ag on Ag/CeO_2 played an important role. It was proposed that O_2 molecules were activated by Ag over Ag/CeO_2, and then rapidly occupied the surface oxygen vacancies with the increase of temperature. It is well accepted that the improvement of OSC of ceria is via reversible oxygen-vacancy formation and partial reduction [42, 43]. Herein, the OSC of Ag/CeO_2 was superior to that of CeO_2, which should be attributed to the larger amount of lattice oxygen of the former taking part in the reaction. The presence of Ag could promote the activated oxygen filled in the oxygen vacancies, which acted as the active sites for the next oxidation reaction.

4 Conclusions

The Ag/CeO_2 catalyst prepared by sol–gel method exhibited much higher activity than pure CeO_2 for CO oxidation. The presence of silver significantly improved the reducibility of surface capping oxygen of ceria. In addition, the inserted Ag increased the crystal defects of CeO_2, which may accelerate the activation of lattice oxygen in the reaction. The Raman results during the reaction processes demonstrated that the release of lattice oxygen led to the formation of oxygen vacancies under CO atmosphere and the resulting vacancies were sealed by oxygen under O_2 atmosphere on Ag/CeO_2 catalyst, which indicated that the presence of Ag improved the OSC of ceria. The obtained results showed that the great increases in the concentration of oxygen vacancies and lattice oxygen were mainly responsible for the higher catalytic activity of Ag/CeO_2 for CO oxidation.

Acknowledgments This work was financially supported by Research Center of Analysis and Test of East China University of Science and Technology. The authors are grateful to Dr. J. X. Li, L. H. Zhou, Y. Q. Song and Professor Y. P. Du for helpful discussions.

References

1. Sayle TXT, Parker SC, Catlow CRA (1992) J Chem Soc Chem Commun 14:977
2. Guzman J, Carrettin S, Corma A (2005) J Am Chem Soc 127:3286
3. Hu ZP, Metiu H (2011) J Phys Chem C 115:17898
4. Trovarelli A (1996) Catal Rev Sci Eng 38:439
5. Reddy BM, Thrimurthulu G, Katta L (2009) J Phys Chem C 113:15882
6. Laguna OH, Sarria FR, Centeno MA, Odriozola JA (2010) J Catal 276:360
7. Hernández WY, Centeno MA, Romero-Sarria F, Odriozola JA (2009) J Phys Chem C 113:5629
8. Yu Q, Wu X, Tang C, Qi L, Liu B, Gao F, Sun K, Dong L, Chen Y (2011) J Colloid Interf Sci 354:341
9. Reddy BM, Katta L, Thrimurthulu G (2010) Mater Chem 22:467
10. Reddy BM, Lakshmanan P, Bharali P, Saikia P, Thrimurthulu G, Muhler M, Gruünert W (2007) J Phys Chem C 111:10478
11. Wang S, Zheng XC, Wang XY, Wang SR, Zhang SM, Yu LH, Huang WP, Wu SH (2005) Catal Lett 105:163
12. Lendzion-Bieluń Z, Bettahar MM, Monteverdi S, Moszyński D, Narkiewicz U (2010) Catal Lett 134:196
13. McBride JR, Hass KC, Poindexter BD, Weber WH (1994) J Appl Phys 76:2435
14. Chen HT, Chang JG (2011) J Phys Chem C 115:14745
15. Taylor SH, Rhodes C (2006) Catal Today 114:357
16. Comsup N, Panpranot J, Praserthdam P (2010) J Ind Eng Chem 16:703
17. Derekaya FB, Güldür Ç (2010) Int J Hydrogen Energy 35:2247
18. Yu L, Shi Y, Zhao Z, Yin H, Wei Y, Liu J (2011) Catal Commun 12:616
19. Imamura S, Yamada H, Utani K (2000) Appl Catal A 192:221
20. Sarode PR, Priolkar KR, Bera P, Hegde MS, Emura S, Kumashiro R (2002) Mater Res Bull 37:1679

21. Scirè S, Riccobene PM, Crisafulli C (2010) Appl Catal B 101:109
22. Bera P, Patil KC, Hegde MS (2000) Phys Chem Chem Phys 2:3715
23. Tang X, Zhang B, Li Y, Shen W (2004) Catal Today 93:191
24. Trovarelli A, Dolcetti G, De Leitenburg C, Santoni A (1992) J Chem Soc Faraday Trans 88:1311
25. Damyanova S, Pawelec B, Arishtirova K, Huerta MVM, Fierro JLG (2008) Appl Catal A 337:86
26. Zhang H, Zhu A, Wang X, Wang Y, Shi C (2007) Catal Commun 8:612
27. Han MM, Wang XJ, Shen YN, Tang CH, Li GS, Smith JRL (2010) J Phys Chem C 114:793
28. Barrabés N, Föttinger K, Llorca J, Dafinov A, Medina F (2010) J Phys Chem C 114:17675
29. Wu P, Zhang H, Du N, Ruan L, Yang D (2009) J Phys Chem C 113:8147
30. Zheng Y, Chen C, Zhan Y, Lin X, Zhu J (2008) J Phys Chem C 112:10773
31. Arabatzis IM, Stergiopoulos T, Bernard MC, Labou D, Neophytides SG, Falaras P (2003) Appl Catal B 42:187
32. Li B, Li H, Xu Z (2009) J Phys Chem C 113:21526
33. Gao J, Arunagiri T, Chen J, Goodwill P, Chyan O (2000) Chem Mater 12:3495
34. Pu ZY, Liu XS, Jia AP, Xie YL, Lu JQ, Luo MF (2010) J Phys Chem C 114:10857
35. Reddy BM, Bharali P, Saikia P, Khan A, Loridant S, Muhler M, Grünert W (2007) J Phys Chem C 111:1878
36. Katta L, Sudarsanam P, Thrimurthulu G, Reddy BM (2010) Appl Catal B 101:101
37. Luo MF, Yan ZL, Jin LY, He M (2006) J Phys Chem B 110:13068
38. Li G, Wang Q, Zhao B, Shen M, Zhou R (2011) J Hazard Mater 186:911
39. Pu ZY, Lu JQ, Luo MF, Long XY (2007) J Phys Chem C 111:18695
40. Shapovalov V, Metiu H (2007) J Catal 245:205
41. Huang M, Fabris S (2008) J Phys Chem C 112:8643
42. Skorodumova NV, Simak SI, Lundqvist BI, Abrikosov IA, Johansson B (2002) Phys Rev Lett 89:166601
43. Trovarelli A (1996) Catal Rev-Sci Eng 38:439